ORIGINAL ARTICLE

DOI: https://doi.org/10.18599/grs.2024.1.2 Russian Original 2024. Vol. 26. Is. 1. Pp. 20–37

Features of Sulfide Mineralization of the Hydrothermal System of Cape Fiolent (Southwestern Crimea)

N.V. Lubnina[1], O.V. Krylov[2], A.Yu. Bychkov[2], I.N. Modin[2], A.D. Skobelev[2], E.V. Kozlova[3], V.L. Kosorukov[2], M.V. Kosnyreva[2], N.I. Kosevich[1,2], A.Yu. Palenov[2]*

[1]*Sevastopol State University, Sevastopol, Russian Federation*
[2]*Lomonosov Moscow State University, Moscow, Russian Federation*
[3]*Skolkovo Institute of Science and Technology, Moscow, Russian Federation*

Abstract. As a result of generalization of geophysical studies, petro-paleomagnetic and structural-geomorphological analyses, as well as thermodynamic modeling, some features of ore formation in the hydrothermal system of Cape Fiolent (southwestern Crimea) under island arc conditions were revealed.

It has been established that the main transformations of rocks of the Middle Jurassic igneous complex of Cape Fiolent occurred under the influence of hydrothermal fluids during the introduction of felsic intrusions during 168–140 Ma. The zones contain sulfide mineralization, the main minerals of which are pyrite, sphalerite, pyrrhotite, galena, chalcopyrite and arsenic pyrite. In the central parts of the hydrothermal alteration zone, massive sulfides are strongly weathered; these zones contain many secondary sulfates. In the marginal parts of hypergenic limonite, yellow-brown goethite prevails in the oxidation zone, yellow jarosite in the center, which is probably due to the large amount of pyrite in the center of the system, which gave more sulfuric acid during oxidation. The presence of native sulfur in the section testifies to the mixing of the acidified hydrothermal solution with seawater. Complex petro-paleomagnetic and magnetometric studies have shown that contact changes and transformation of the contrasting basalt-rhyolite formation occurred along the NNW-trending faults.

Keywords: hydrothermal system, sulfide mineralization, petro-paleomagnetism, electrotomography, magnetometry, faults, island arc

Recommended citation: Lubnina N.V., Krylov O.V., Bychkov A.Yu., Modin I.N., Skobelev A.D., Kozlova E.V., Kosorukov V.L., Kosnyreva M.V., Kosevich N.I., Palenov A.Yu. (2024). Features of Sulfide Mineralization of the Hydrothermal System of Cape Fiolent (Southwestern Crimea). *Georesursy = Georesources*, 26(1), pp. 20–37. https://doi.org/10.18599/grs.2024.1.2

Introduction

Recently, research on underwater hydrotherms has become in demand both from a practical and a scientific point of view. Special attention is paid to the study of hydrothermal systems of island arcs, since the formation of the majority of ancient pyrite objects is connected precisely with the island arc regime (de Ronde et al., 2011; Fouquet et al., 2018; Keith et al., 2021; Stoffers et al., 2006). It is shown that hydrothermal activity is widespread on active submarine volcanoes of island arcs and, as a rule, is confined to the peripheral parts of the of submarine volcanoe calderas (Stix et al., 2003). Ore formation occurs due to a sharp drop in temperature when the hydrothermal solution mixes with cold bottom water, and the composition of the crust substrate is the decisive factor for ore formation, as well as the participation of magmatic fluids in the supply of hydrothermal systems (Grichuk, 2012).

The origin of the Black Sea deep-water basin is associated with the formation of a back-arc basin with an oceanic-type crust behind the Cretaceous Pontides volcanic arc (Afanasenkov et al., 2007; Okay et al., 1994; Nikishin et al., 2015, etc).

Proposed by V.V. Yudin new geodynamic model of Crimea (Yudin, 2011) suggests the existence of a Jurassic-Lower Cretaceous forearc collisional suture with a melange composed of dynamometamorphic formations and fragments of the oceanic crust of the ancient MesoThetis ocean. Traced at the base of the Main Range, the Podgorny and Yuzhnoberezhny melanges are recognized as active structures of Neogene-Quaternary time (Yudin, 2011).

Two main tectonic areas are distinguished in Crimea: (1) the Scythian platform with a Paleozoic foundation

*Corresponding author: Natalia V. Lubnina
e-mail: natalia.lubnina@gmail.com

in a steppe Crimea; (2) South-Crimean orogen and the regional molasses basins associated with it in the Kerch-Taman area.

In the South-Western part of the Crimean peninsula within the limits of the Herakleian Plateau on the Cape Fiolent, sulphide mineralization is first mentioned in the works of S.P. Popova (1913) and P.A. Dvoichenko (1914). Sulfide mineralization in Crimea is considered in work (Borisenko et al., 1981). The Herakleian ore profile was studied in the most detailed manner during the State geological mapping program (Pivovarov et al., 1984). A summary of the gold-silver and sulfide mineralization in the rocks of the Herakleian plateau is presented in the work of E.F. Shnyukov and co-authors (Shnyukov et al., 2008), who showed that these ore manifestations represent medium- and low-temperature hydrothermal formations.

However, the questions of time and location of the hydrothermal system, its configuration and connection with ore exposure, still remain discussed.

For the identification of spatial-temporal regularities in the manifestation of the hydrothermal system in 2017−2021 on the Cape Fiolent, a complex geological-geophysical study of the features of the sulfide mineralization of the hydrothermal system of the Cape Fiolent was carried out, including materials from electrotomographic (1 profile), magnetometric (3 profiles), gravimetric (1 profile), hydromagnetic (1 profile) studies, petro- and paleomagnetic data on 70 samples, as well as the results of X-ray phase (13 samples) and microprobe (1 sample) analyses.

Geological structure of the study area

The Herakleian Plateau is an isolated volcanic tectonic block in the suture zone of the junction of the Scythian Plate and the Mountain Crimea (Geology of the USSR..., 1969). From the southeast it is bounded by the Georgievskaya zone of faults (en echelon tectonic disturbances), active in the late Alpine stage, and from the northeast by the early Kimmerian zone of deep-seated faults (Fig. 1). This region belongs to the junction zone of three structures: the Scythian Plate, the Mountain Crimea and the Western Black Sea Basin and is characterized by a continental basaltic crust that thins in the direction from the land to the center of the basin (Borisenko et al., 1981; Shatalov, 1999; Shnyukova, 2005, etc.).

In its structure, the upper and lower structural floors are distinguished (Fig. 2).

The lower structural floor is composed of Middle Jurassic volcanic deposits. In the Cape Fiolent area, they are described as an ophiolitic association, including serpentinized ultrabasics and serpentinites, a layered basic-ultrabasic complex, gabbro and gabbro-dolerites, fragments of a complex of parallel dikes, pillow lavas, siliceous black layered formations and jasper. The chemical composition, including the distribution of rare earths elements and a wide spectrum of other microelements, of pillow lavas and dolerites from the ophiolites of the Cape Fiolent, indicates their suprasubduction nature and belonging to a back-arc basin that has reached the spreading stage in its development (Promyslova et al., 2014). These rocks are pierced by extrusive domes, bosses and dikes of plagioriolites.

Plagioriolites are porphyry rocks of light-green-gray color. Porphyry inclusions up to 1.5–2.0 mm in size are represented by tabular acidic plagioclase and isometric quartz crystals embedded in a cryptocrystalline quartz-plagioclase groundmass (Promyslova et al., 2014). According to their petro-geochemical characteristics,

Fig. 1. Tectonic scheme of the southern margin of the East European Platform (modified after Nikishin et al., 2015). The red dotted line on the map marks the boundary of the foothill collision structure. The inset shows the position of the Heracleian Plateau. The dotted lines show the Chernorechensky and Georgievsky faults

Fig. 2. General view of the outcrops of Middle Jurassic igneous rocks (lower structural level) in the area of the Cape Fiolent and the overlying Miocene deposits (upper structural level). The dotted line marks the stratigraphic contact between the upper and lower structural levels. Inset A is a diagram of the geological structure of the Heracleian Peninsula (modified after Geology of the USSR..., 1969 and Promyslova et al., 2019). Legend: 1 – modern deposits: sands, pebbles, clays, loams; 2 – Upper Miocene deposits, Sarmatian regional stage: clays, limestones, sandstones; 3 – Paleocene deposits: terrigenous-clayey-carbonate strata; 4 – Cretaceous deposits: carbonate-terrigenous and tuffaceous-clayey strata; 5 – Upper Jurassic deposits: carbonate and clayey-terrigenous strata; 6 – Middle Jurassic (Bajocian) igneous complexes of the Cape Fiolent; 7 – second-order deep faults, the Georgievsky Fault; 8 – second-order faults dividing the Heracleian Plateau into Western, Central and South-Eastern segments; 9 – coastline

plagioriolites belong to low- or moderate-potassium siliceous rocks of the lime-alkaline series with a moderate distribution spectrum of rare earth elements and a well-recognized negative Eu anomaly (Kuznetsov et al., 2022; Promyslova et al., 2014). According to U-Pb-dating data on zircons (SHRIMP-II, VSEGEI, Saint-Petersburg), the age of plagioriolites is determined as 168.3 ± 1.3 million years (Kuznetsov et al., 2022).

In early interpretations V.V. Yudin, in the southern part of the Herakleian plateau, the Fiolent volcano, associated with the Fiolent and Chersonese deep fault-thrusts, was isolated (Yudin, 1995).

Deformation of the lower structural layer occurred before the deposition of the Lower Cretaceous and younger sedimentary cover, which is weakly or almost not deformed.

Along the southern shore of the Herakleian Plateau, a stratigraphic contact is exposed between the Middle Jurassic volcanic deposits of the lower structural layer and the Upper Miocene limestones of the upper structural layer with a well-defined basal horizon (white dashed line on Fig. 2).

The upper structural floor is composed of Early Cretaceous – Miocene rocks. However, within the limits of the Herakleian Plateau, the lower Cretaceous sequence is wedged out in a southwest direction, often with complete erosion of Upper Cretaceous and Paleogene rocks (Geology of the USSR..., 1969), and only the limestones and clays of the Lower Neogene (Sarmatian regional stage of the Upper Miocene), which lie subhorizontally and form the plateau, upper structural floor. The total thickness of the Miocene sediments reaches 30–40 m.

A great importance in the structure of the region is played by discontinuous disturbances of various orders, the formation of which to a significant degree predetermined its structural features. According to their parameters and role in geological history, discontinuities are divided into deep first-order faults, deep-seated second-order faults and local third-order discontinuities of different morphology (Pivovarov et al., 1984 and bibliography therein). 1st order faults, mainly developed, according to gravity exploration data, in angular Permian rocks, have north-northwest and east-northeast trends and are not expressed in any way in Middle Jurassic and modern structural plans (Pivovarov et al., 1984).

Deep-laying second order faults represent the same type of faults of the NW and NE trends. They are distinctly distinguished according to the data of magnetic prospecting in the Middle Jurassic volcanic sequence (Golubev et al., 1976), and in Miocene deposits based on the data of vertical electrical sounding (VES) and inducted polarization (IP) (Litvinov, Golubev, 1983), creating a block structure (Yudin, 1995). At the same time, the displacement of faults in the Middle Jurassic plane in relation to the Miocene one sometimes indicates the direction of the displacement (Pivovarov et al., 1984; Murovskaya, Shcherbakov, 2011).

The previously carried out structural-geomorphological studies within the Herakleian Peninsula (Fig. 3) made it possible to distinguish the Western, Central and South-Eastern segments, which differ in the density and direction of fracture zones, discontinuities of the third-order, the nature of the ravine-

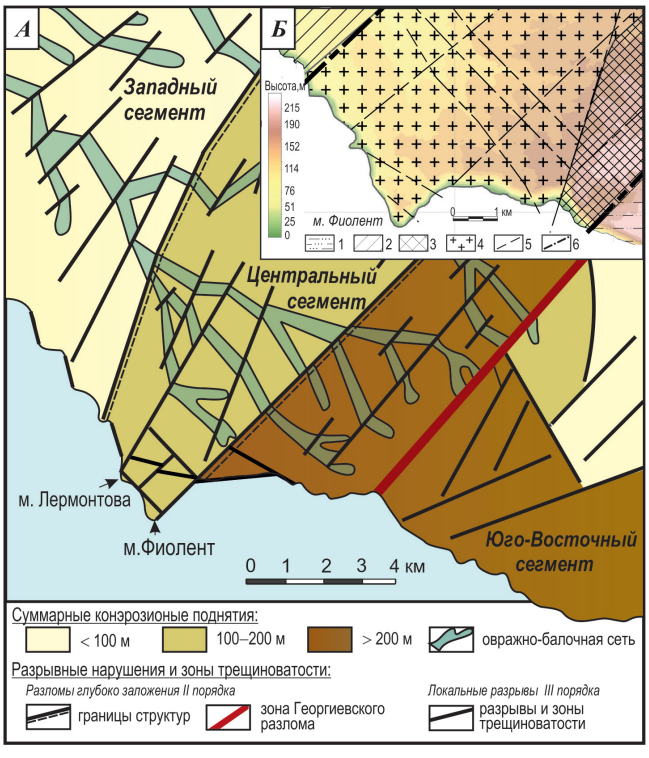

Fig 3. Structural and geomorphological map of the Cape Fiolent and adjacent territories (44°30'3.05" N and 33°29'34.76" E) modified after (Lubnina et al., 2022) (A); Inset B is a diagram of the main tectonic faults and geodynamic settings of the South-Western Crimea on the relief map modified after (Ivanov et al., 2009). Symbols: 1 – Balaklava macroblocks; 2 – relatively stable areas of the Heracleian Plateau; 3 – zone of the Georgievsky fault; 4 – sections of the Heraclean plateau in effected zone of the Georgievsky fault, subject to intense dislocations; 5 – main tectonic faults; 6 – tectonic lineaments

gully net, the structure of the coastal zone (Promyslova et al., 2019). The boundaries of these segments are marked by large extended faults of the second-order NNE-strike (Fig. 3).

For the Western segment, there is a characteristic system of cracks of the third-order, mainly in the north-western direction, which is developed by a ravine-gully net. Most of the beams form deep cuts with several exposed edges, in the central parts of the beams a graben-like structure is shown (Krylov et al., 2023).

In the central segment, a wide development has a zone of tectonic disturbances of the third-order ENE-trend. On the Cape Fiolent, the largest NE-fracturing zone is identified. It's bordered of two segments – the Central one with a relief, significantly divided by the ravine-gully net, and the South-Eastern one with undivided relief. In the Central segment, numerous fractures deform the valleys of ravines and gullies, changing their direction (Fig. 3).

In the South-Eastern segment, where significant influence of the Georgievsky Fault is observed, third-order fractures and ruptures predominate, with NE-trends of 30–40° and 60–70° (Ivanov et al., 2009). NW-trend fractures are practically absent (Fig. 3).

Cape Fiolent hydrothermal system (44°30'3,05" N 33°29'34,76" E)

Hydrothermal system has been investigated at 1 km SE of the second order Fiolent fault, at the eastern edge of the Cape Fiolent. It's corresponded to the NE fault, identified according to the VES data in the Middle Jurassic volcanic sequence (Pivovarov et al., 1984). According to Borisenko, the NE-trended fault crossing the volcanogenic formation is expressed by zone of fragmentation, hydrothermal processing and the intrusion of a felsite dike (Borisenko et al., 1981).

We studied a fragment of a hydrothermal system 400 m NE of the Cape Fiolent in the coastal cliffs, where two subvertical lit zones of metasomatically altered rocks containing pyrite stock are exposed (Krylov et al., 2023). Metasomatic changes develop both along fractures in Middle Jurassic pillow basalts and at the contact with plagioriolites.

Contact zones of plagioriolitic intrusions and intervening pillow basalts have been transformed into light porcelain rocks with relicts of isometric high-temperature quartz grains. The color of the metasomatites is due to the different intensity of silicification and the different amount and composition of limonite, which develops on pyrite. The zone of metasomatic changes has a clearly expressed zonal structure.

To determine the composition of altered rocks in different parts of this zone, an X-ray phase analysis was carried out on an X-ray diffractometer MiniFlex 600 (Rigaku, Japan) at Faculty of Geology of Lomonosov Moscow State University (MSU). For the study the weighted sample (3.0 g) were rubbed to the state of a fine powder (about 0.01 mm). They filled a cuvette with a diameter of 20 mm and a thickness of 2 mm with the obtained powder and took a picture on a diffractometer with an X-ray tube with a copper anticathode at a working current of 15 mA and a working voltage of 40 kV. The resulting diffractogram was processed using the MATCH program, the mineral phases contained in the sample and their percentage content in the sample were determined. The results of X-ray phase analysis are shown in Table 1 and on Fig. 4.

Microprobe studies of the mineralogy of sulphide veins performed on an SEM model JSM-6480LV (Jeol, Japan) in MSU. Local quantitative analysis of the chemical composition of minerals was carried out using an attachment for energy-dispersive X-ray microanalysis INCA Energy 350 (Oxford Instruments, UK) (analyst V.O. Yapaskurt).

A mineralogical association of pyrite, pyrrhotite, sphalerite, chalcopyrite, galena characteristic of pyrite

Composition, %	Sample number												
	Central part					Marginal parts						Contact	
	K_{18}	K_1	K_{1p}	K_{26}	K_{26p}	K_3	K_{3a}	K_{24}	K_8	K_9	K_{11}	K_2	K_4
Mica	–	–	–	–	–	11	4	2	18	–	4	–	1
Quartz	25	–	–	35	–	13	19	44	38	10	30	17	8
Plagioclase	57	45	–	8	–	–	–	18	–	1	–	–	–
Calcite	5	5	–	–	–	–	–	–	–	–	–	–	–
Sulfur	–	–	–	–	–	–	–	–	–	–	–	–	–
Chlorite	–	4	–	1	–	–	–	4	–	1	–	–	–
Gypsum	1	–	7	1	5	4	6	3	2	31	29	28	–
Jarosite	–	–	–	3	–	34	3	17	–	52	21	–	–
Sulfides	7	11	–	1	–	36	68	11	42	5	16	55	91
Smectite	5	–	–	–	–	2	–	1	–	–	–	–	–
Microsommit	–	25	–	38	–	–	–	–	–	–	–	–	–
Basalumite	–	10	–	13	3	–	–	–	–	–	–	–	–
Alunogen	–	–	87	–	92	–	–	–	–	–	–	–	–
Zaherit	–	–	3	–	–	–	–	–	–	–	–	–	–
Total	100	100	100	100	100	100	100	100	100	100	100	100	100

Table 1. Results of X-ray phase analysis of samples from the "pyrite stockwork" on the Cape Fiolent. Bulk samples

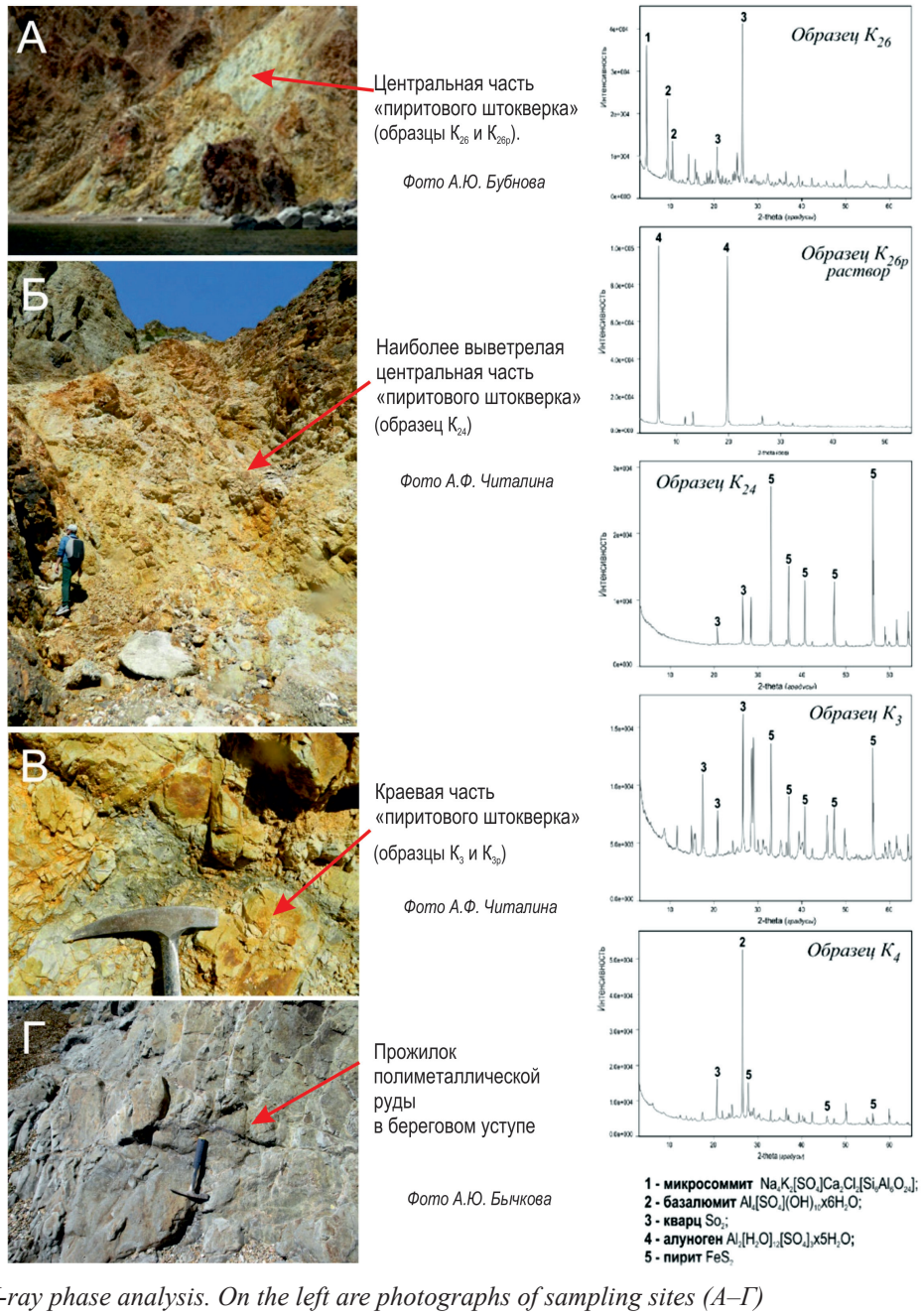

Fig. 4. Results of X-ray phase analysis. On the left are photographs of sampling sites (А–Г)

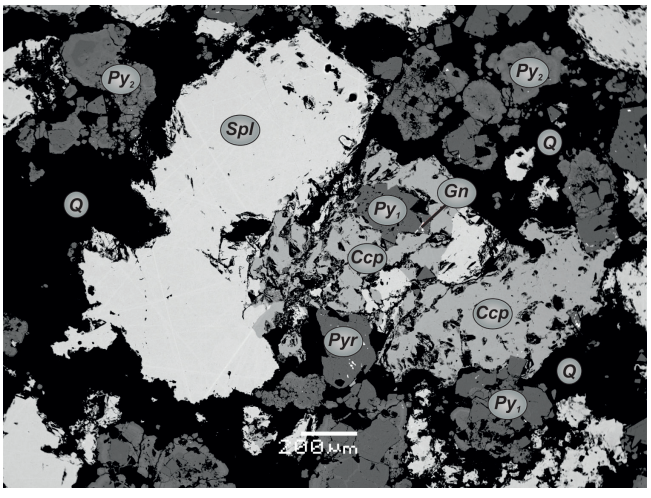

Fig. 5. Back electron image of sample K18-24. Designations: Q – quartz, Spl – sphalerite, Py – pyrite (Py1 and Py2 – first and second generations, respectively), Pyr – pyrrhotite, Ccp – chalcopyrite, Gn – galena

deposits has been established (Fig. 5). Two generations have been identified for pyrite. The first one is an early generation, represented by well-formed cubic crystals with a composition close to the theoretical one, practically without impurities. Single grains of pyrrhotite are associated with it. The second generation is represented by collomorphic zonal separations. Pyrite of the second generation contains arsenic up to 5.6 mas. %, silver until 1 mas. %, copper up to 0.4 mas. % and antimony up to 0.3 mas. %. Pyrite deposition of the second generation occurred after the formation of sphalerite and chalcopyrite. Galena in the sample met in the form of a single grain. Sphalerite contains 2.2–2.6 mas. % of Ferrum and 0.3–0.4 mass. % of cadmium.

The sequence of mineral deposition can be represented by three stages. At the first, an association of pyrite and pyrrhotite was formed, at the second, the deposition of the main ore minerals: sphalerite and chalcopyrite (possibly also galena), at the third stage, arsenic pyrite was formed, which often grows on pyrite of the first generation and minerals of the second stage.

According to the association of minerals, the fragment of the ore hydrothermal system corresponds to the pyrite type, which is characteristic of the contrasting basalt-rhyolite formation.

In the hypergenic limonite, yellow-brown goethite predominates in the oxidation zone of the "pyrite stock", and in the center – yellow, which is probably due to the greater content of pyrite in the center of the system, which during oxidation released more sulfuric acid.

In the central parts, massive sulfides are strongly weathered, these zones contain many secondary sulfates (Fig. 4Б).

As a result of X-ray phase analysis, such secondary minerals as gypsum, jarosite, microsommite and basalumite were established. These minerals are characteristic of weathering zones of volcanic deposits in the Mediterranean climate. The presence of secondary sulfates testifies to the fact that sulphide veins emerging on the surface are experiencing active contemporary weathering.

Geophysical survey included petro- and paleomagnetic, magnetometric, gravimetric and electrotomographic studies (Fig. 6). Two-dimensional magnetic and density modeling were carry out to confirm the origin of magnetic and gravity anomalies.

During the fieldwork, measurements of magnetic susceptibility were carried out with KT-5 kappameter in coastal cliffs, which made it possible to type the section and select objects (sites) for detailed petro- and paleomagnetic testing. The sampling scheme and the position of the sites are shown in Fig. 6.

When selecting a collection of samples for petro- and paleomagnetic studies, their orientation in space was performed using magnetic and solar compasses. For laboratory studies, cubes 2 cm^3 were cut out of all samples.

Petro-paleomagnetic studies carried out in the Petromagnetic laboratory of MSU according to the standard procedure (Khramov et al., 1982) and included magnetic cleaning (alternating field and stepped temperature). NRM components were visually identified by using stereographic and orthogonal projections (Zijderveld, 1967). The directions of components were calculated by principal component analysis method (Kirschvink, 1980). Mean directions were calculated according to Fisher (1953). All calculations and graphic representations of the results were performed using Remasoft 3.0 software (AGICO, Czech Republic). To evaluate the magnetic stability of the sample, we used the Königsberger ratio (factor Q). Thermomagnetic measurements (magnetic susceptibility versus temperature, K/T curves) were carried out for one sample from each of the the main petrological differences of the magmatic complexes of the southwestern Crimea. Each Curie temperature (Tc) shown in the K/T curve characterizes a ferromagnetic mineral or phase in the rock.

Magnetometric studies on the Cape Fiolent were carried out using a quantum magnetometer Geometrics G-858 (Geometrics, USA). Magnetometric observations were carried out along four profiles with an azimuth of 58° NE (profiles MMP1–MMP4 on Fig. 6). The central profile coincided with the profile of the electrotomographic (ET) and gravimetric works (GRR), the distance between the profiles was 50–60 m and was determined by the possibilities of movement on the terrain without significant disturbances.

The length of the profiles was taken at 600–800 m, the linking of the observation points was carried out with the help of a GPS satellite receiver-navigator. According to the data of the GPS height measurement during all the movements during the work, a relief map was constructed (Fig. 6).

Measurements of the magnetic field along the profiles of the work were made every 15–20 cm, which allowed to reject anomalies associated with man-made iron debris and structures. For the calculation of the anomalous magnetic field, they introduced corrections for the variations and found the value of the normal magnetic field. Variations of the geomagnetic field were registered at a field magnetic variation station located directly on the site of the work. In the quality of the station, a proton magnetometer was used MMPOS-1 (LLC Proton SPb, Russia) with a registration period of 6 s.

Due to the small size of the research area, the normal magnetic field was calculated according to the IGRF-13 model (Alken et al., 2021). Since all measurements of the magnetic field were carried out only along 4 parallel profiles, maps of the anomalous magnetic field were not constructed, the data were analyzed in the form of graph maps and maps of classified points.

Magnetometric studies were compared with the results of previous magnetometric (Pivovarov et al., 1984) and hydromagnetic (Isaev et al., 2018) studies in the area of the Cape Fiolent.

Identified magnetic anomalies because of ground and marine works were matched with structural-geomorphological and tectonic maps (Ivanov et al., 2009; Lubnina et al., 2021; Krylov et al., 2023).

Gravimetric studies were carried out with a high-precision gravimeter CG-5 Autograv (SCINTREX, Canada). Sensor type – fused quartz with electrostatic compensation. Automatic correction – tide, inclination of the device, temperature, noise suppression, seismic filter. The accuracy of the gravimetric survey was 3 μGal. These works were accompanied by planar and high-altitude anchorages of observation points, carried out with Sokkia tacheometer (Sokkia Topcon Co., Ltd., Japan). The accuracy of the height at the points of the gravimetric network was 1 cm, planar coordinates – 5 cm.

The length of the gravimetric profile was 400 m with steps 10 m (Fig. 6). As a point of support, a row picket with number 97 was chosen. To assess the accuracy of the gravimetric survey, control observations were

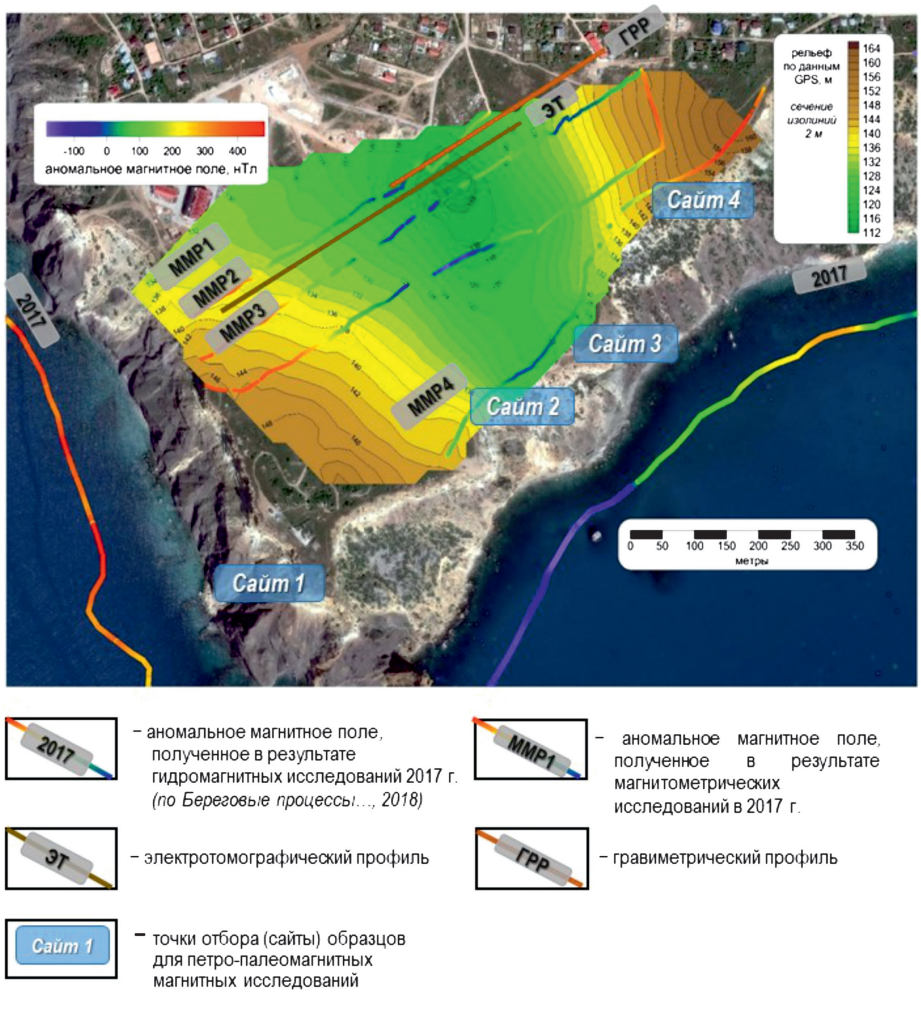

Fig. 6. Geophysical and rock magnetic studies carried out in 2017–2021 field works on the Cape Fiolent

carried out at 20% of the total number of ordinary points. The processing of gravimetric observations included the introduction of corrections for: (1) sliding of the zero-point gravimeter; (2) accounting for lunar-solar variations of the Earth's gravitational field; (3) the normal value of the force of gravity according to the G. Helmert formula; (4) corrections for free air and the attraction of the intermediate layer. As a result of the processing, a catalog of the values of gravity at the points of the row network was obtained and the gravity anomaly was calculated in the Bouguer reduction with the density of the intermediate layer of 2.3 g/cm^3.

Electrotomographic studies were carried out along one profile with a length of 735 m (ET on Fig. 6) at the Omega-48 equipment complex (LLC Logis, Russia). Dipole axial and symmetric inverse four-electrode installations were used to increase the stability of the inversion procedure. The distance between the electrodes was 5 m, the maximum distance between the electrodes was 87.5 m, which provided a depth of about 40 m. The length of one layer was 235 m, and the layers adjacent to the profile were carried out with a 50% overlap, which allowed to obtain a continuous profile with a given depth and to estimate the accuracy of the measurements on the layers at different intervals. Thus, five layouts were made, which correspond to the five positions of the electrotomographic station on the observation profile. Total number of measurements on the profile is 3135.

The two-dimensional inversion of the data and the selection of the optimal inversion parameters were carried out using the RES2DINV software. In the result of electrotomographic studies, a geoelectrical plot was constructed with the accuracy of 4.2%.

Geoelectrical boundaries were distinguished by zones of maximum gradient of electrical resistivity (ER) both laterally and in depth. Areas on the geoelectric section with ER values above 500 Ω·m were related to blocks of dense undisturbed limestones, complexes with values of 200–500 Ω·m were distinguished as weakly- and medium-cracked limestones, and with values of 70–120 Ω·m – as strongly cracked limestones with increased porosity and clay. Areas of the geoelectrical section with ER values less than 20 Ω·m were interpreted as zones of increased fracturing and secondary mineralization.

2D magnetic and gravity modeling was performed in the author's program complex TM-2D/TG-2D (Bulychev, Zaitsev, 2008a; 2008b), intended for the solution of the problem of selecting anomalous fields of cracks given by a system of closed polygons with constant magnetization/density in profile variation. The program gives the opportunity to change the parameters of the section (Azimuth of the profile, normal field, declination, inclination in the variant of magnetic modeling) and the parameters of each body (module of magnetization, declination, inclination, density) in an interactive mode.

The density and magnetic models were built in a single concept of a two-tier structure, where the upper layer is Miocene limestone with variable density (2.6–2.7 g/cm^3) and zero magnetization. The roof of the limestone corresponds to the daytime relief, and as a sole, the lower border of the limestone, selected according to the results of electrotomographic studies, was used. The lower layer is represented by Middle Jurassic magmatic complexes, the roof of which corresponds to the base of the Miocene limestones. In the magnetic model, the sole of the lower layer is limited by the horizontal boundary at a depth of 800 m, in the density model at a depth of 400 m, in accordance with the lengths of the profiles. The selection of density and magnetism, as well as the determination of the position and inclination of the subvertical boundaries, were carried out mainly within the lower tier. We note that the selection of subvertical blocks within this layer was carried out with the support of photo-decoding of exposures on the eastern shore of Cape Fiolent. As the starting values of the module and the angle of magnetization, the data of petromagnetic studies performed on the exposures of the investigated section were used.

Results

Petro- and paleomagnetic magnetic studies. The Upper Miocene limestones are weakly magnetic. The values of natural remanent magnetization (NRM) and magnetic susceptibility (χ) are maintained laterally and do not exceed (0.01–2.03) 10^{-3} A/m and (0.05–0.7) 10^{-3} SI, respectively. According to thermomagnetic analysis, the main mineral carrier of magnetization is greigite. The clayey layers are the most magnetic in the section. The samples exhibit a two-component composition of NRM. The low-temperature component coincides with the direction of the present-day geomagnetic field (PDF) in this work area, the high-temperature component (SM) has NNE steep downward directions (Table 2).

The studied magmatic complexes of the lower structural level can be divided into three main groups.

Group I. The most magnetic are the Middle Jurassic pillow basalts, the value of magnetic susceptibility varies from $7.5 \cdot 10^{-3}$ to $15.6 \cdot 10^{-3}$ SI. In this case, a "primary" distribution of the magnetic fraction in the rocks is observed – χ increase from contact ((7.5–7.9) 10^{-3} SI) to the central ((12.6–15.6) 10^{-3} SI) parts of pillow. The NRM value varies from 0.3 to 0.82 A/m. Titanomagnetite with T_c 520–545 °C is the main magnetic carrier in unbaked pillow basalts (Fig. 7, sites 1–4).

In unbaked and baked pillow basalt, close to plagiorhyolites, the Tc increases up to 600–620 °C. During stepwise thermal and AF-demagnetizations, two magnetization components were identified. The first

Rock type	χ, 10^{-3} SI units	NRM, A/m	ID	Metachronous component			
				N	*D*, °	*I*, °	α_{95}
Upper structural level. Miocene limestones of the Sarmatian regional stage							
Limestones	0.05–0.7	$(0.01–0.23)\cdot10^{-3}$	SM	15	7.4	63.1	5.9
Lower structural level. Middle Jurassic igneous complexes							
Pillow basalts	8.6–16.9	0.3–0.82	PB	12	24.3	57.0	4.5
Altered pillow basalts	1.36–5.8	0.1–0.48	PC	16	6.4	50.2	4.1
Plagiorhyolites	7.5–12.3	0.1–0.53	PL	11	26.7	55.9	4.6
Hydrothermal alteration zone	0.1–1.0	0.05–0.13	HT	15	9.4	45.0	7.6
"Pyrite stockwork"	0.01–0.03	0.01–0.03	ST	Only paramagnetic fraction			

Table 2. Results of paleomagnetic studies of rocks on the Cape Fiolent

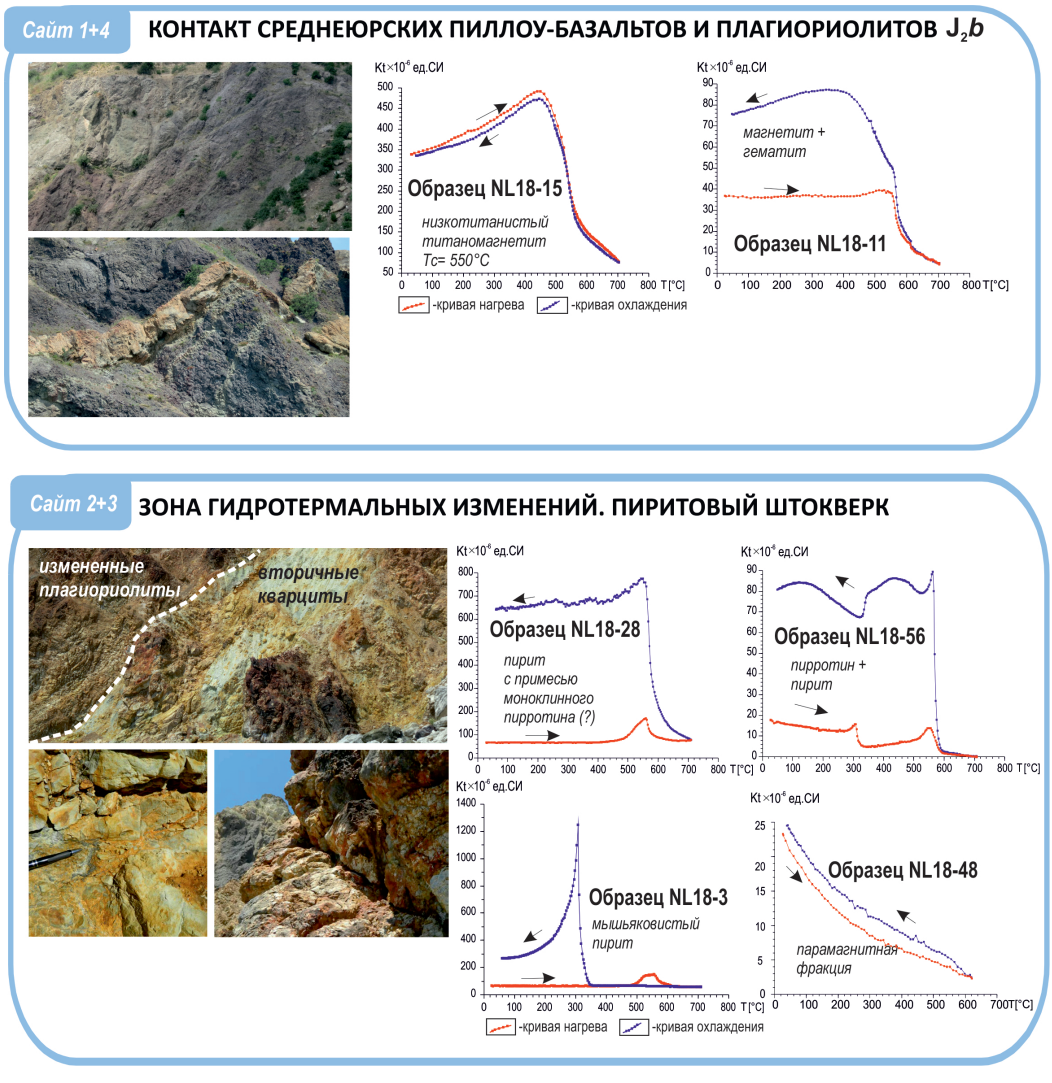

Fig. 7. Results of petromagnetic studies of samples of the hydrothermal system on the Cape Fiolent. See text for explanations

component is close to the PDF. The second high-temperature component (PB) have been isolated by demagnetizations due to either heating at 500–600 °C or after 30–100 mT of the AF treatment. The component has NE intermediate downward direction. Mean direction of the PB component see in Table 2.

Group II. At the SW end of the Cape Fiolent, Middle Jurassic pillow basalts are intruded by plagiorhyolite dikes. The value of χ of plagiorhyolites in this part of the section is $(2.8–5.6)\cdot10^{-3}$ SI, the value of NRM is 7.5–12.3 A/m. In plagiorhyolite samples, two magnetization components are also distinguished. In the temperature range up to 350 °C, a NNE intermediate downward direction coincides with the PEF in the work

area. The second component (PL) of NE intermediate downward direction is distinguished in the temperature range of 450–600 °C (Table 2). The percentage of the high-temperature component in plagiorhyolite samples does not exceed 60%.

III group. At the contact between plagiorhyolites and pillow basalts, a zone of hydrothermal reworking is observed. In general, the zone is characterized by reduced values of magnetic susceptibility, lying within the sensitivity range of the KT-5 – $(0.01–0.03)\cdot10^{-3}$ SI. This zone correlates well with negative magnetic anomalies identified during hydromagnetic and magnetometric studies (Fig. 6, site 2–3). However, detailed studies of magnetic susceptibility and thermomagnetic analysis made it possible to identify a number of patterns in the distribution of the magnetic fraction in this part of the section.

In samples from the central part of the "pyrite stockwork" (alterated quartzites), a predominantly paramagnetic fraction is found (Fig. 7), which does not contain residual magnetization (Q < 1). The value of χ is $(0.01–0.03)\cdot10^{-3}$ SI, NRM value – 0.01–0.03 A/m (Table 2). Thermomagnetic and X-ray diffraction data, as well as microprobe studies, indicate the presence of large amounts of pyrite, as well as chalcopyrite, sphalerite and galena in the rocks, while sulfide mineralization is controlled by northwest-trending faults. Fault zones also correlate well with linearly elongated negative magnetic anomalies established during magnetometric studies (Pivovarov et al., 1984; Krylov et al., 2023). Magnetic minima in the MMP1–MMP4 and GM2017 profiles are associated with these same zones (Fig. 6).

In addition to pyrite, large amounts of monoclinic and hexagonal pyrrhotite were identified in samples from pyrite veinlets. Such samples contain inductive magnetization (Q > 1) and are suitable for paleomagnetic studies. In the southwestern part of the "pyrite stockwork", a zone of hydrothermal processing was discovered containing secondary arsenic pyrite (Fig. 4, 7). The value of magnetic susceptibility is $(0.1–1.0)\cdot10^{-3}$ SI, NRM value – 0.05–0.13 A/m. The samples contain a high-temperature component of LT, which is destroyed at temperatures up to 580 °C. The share of this component in the samples does not exceed 45%. Mean direction of this component is shown in Table 2.

Magnetometric studies. The magnitude of the anomalous field ΔT_a along the central MMP2 profile varies from –190 nT in the central part of the profile (picket 350) to +470 mT in its southwestern part (Fig. 8А, Б). On the map of anomalous magnetic field graphs, the negative zone located in the central part has symmetrical values from –10 to –190 nT (pickets from 310 to 430 in Fig. 8).

The negative zone separates two symmetrical positive zones with a gradient of 12 nT per 10 m (pickets 190–310 in the southwestern part of the profile and 410–460 in the northeastern part). However, in the southwestern direction there is a step where the magnitude of the anomalous magnetic field does not change at a distance of ~ 40 m and is 10–12 nT (Fig. 8Б).

Starting from picket 190, the magnitude of the anomalous magnetic field strength ΔT_a continues to increase in the southwestern direction, reaching values of 490–510 nT near the coastal ledges of the Cape Fiolent with a gradient of 10–15 nT per 10 m. In the northeastern direction, the magnitude of the anomalous magnetic field remains unchanged over 250 m (ΔT_a ~ 100–120 nT). A sharp increase in the strength of the anomalous magnetic field is observed in the area of pickets 750–800 (gradient of 12 nT per 10 m), while the maximum values of ΔT_a (220–250 nT) are lower than in the southwestern part of the section (Fig. 8Б).

Comparison of two positive zones in the very west of the cape and in the northeastern part of the study area according to three magnetometric profiles MMR1–3 (Fig. 6) and the zones of reduced anomalous magnetic field separating them allows us to identify their general northwestern strike (320° NW, Fig. 6, 8).

Despite the general correlation of the anomalous magnetic field and the relief of the daytime surface according to GPS data, it can be noted that the minimum in the relief is shifted relative to the minimum of the magnetic field (Fig. 6).

Gravimetric studies. The geological exploration profile for gravity exploration works coincides with the profile for electrical tomographic studies, its length is 400 m with a step of 10 m (Fig. 8). The accuracy of the gravimetric survey was ±0.002 mGal, and the accuracy of height determination was ±1cm (Fig. 8).

As a result of the research, a graph of the gravitational field in the Bouguer reduction was constructed (the density of the intermediate layer is 2.3 g/cm^3). The maximum values (up to 3.5 mGal) were obtained in the central part of the profile in the area of picket 400 and coincide with the minimum in the relief (Fig. 8Б).

The central part of the profile is characterized by a high gradient (0.05 mGal per 10 m) and a decrease in the values of the gravity field in the northeast direction between pickets 480 and 650. At the edges of the profile, a change in the magnitude and sign of the gradient is expected.

In the area of pickets 400 and 700, positive local anomalies of the same amplitude of 0.05 mGal can be identified. According to electrotomography data, in the area of the same pickets at a depth of more than 30 m, it is possible to identify the boundaries of an area with reduced resistance.

Electrotomographic studies. A profile 715 m long is attached to a beam, the transverse dimensions of which approximately correspond to the length of the profile

(ET profile in Fig. 6). The absolute elevations of the Earth's surface in the northeastern and southwestern parts of the beam are raised to a height of 156 and 146 m, respectively. The total depth of the obtained geoelectric section was 40–50 m. The entire research profile from the point of view of geoelectric structure can be divided into two conductive layers (Fig. 9).

The upper layer is represented by highly differentiated rocks, the resistivity of which varies from 10 to 600 Ohm·m. The thickness of the layer varies from 10 to 25 m. There is an increase in the resistivity of rocks in the southwestern direction, while the geoelectric section becomes more uniform (Fig. 9).

In the northeastern side of the ravine from the thalweg of the ravine (zone III in Fig. 9A), at a distance of about 240 m north of picket 400, a conductive layer is distinguished, the resistivity of which is about 7–8 Ohm·m. The thickness of the conductive layer gradually

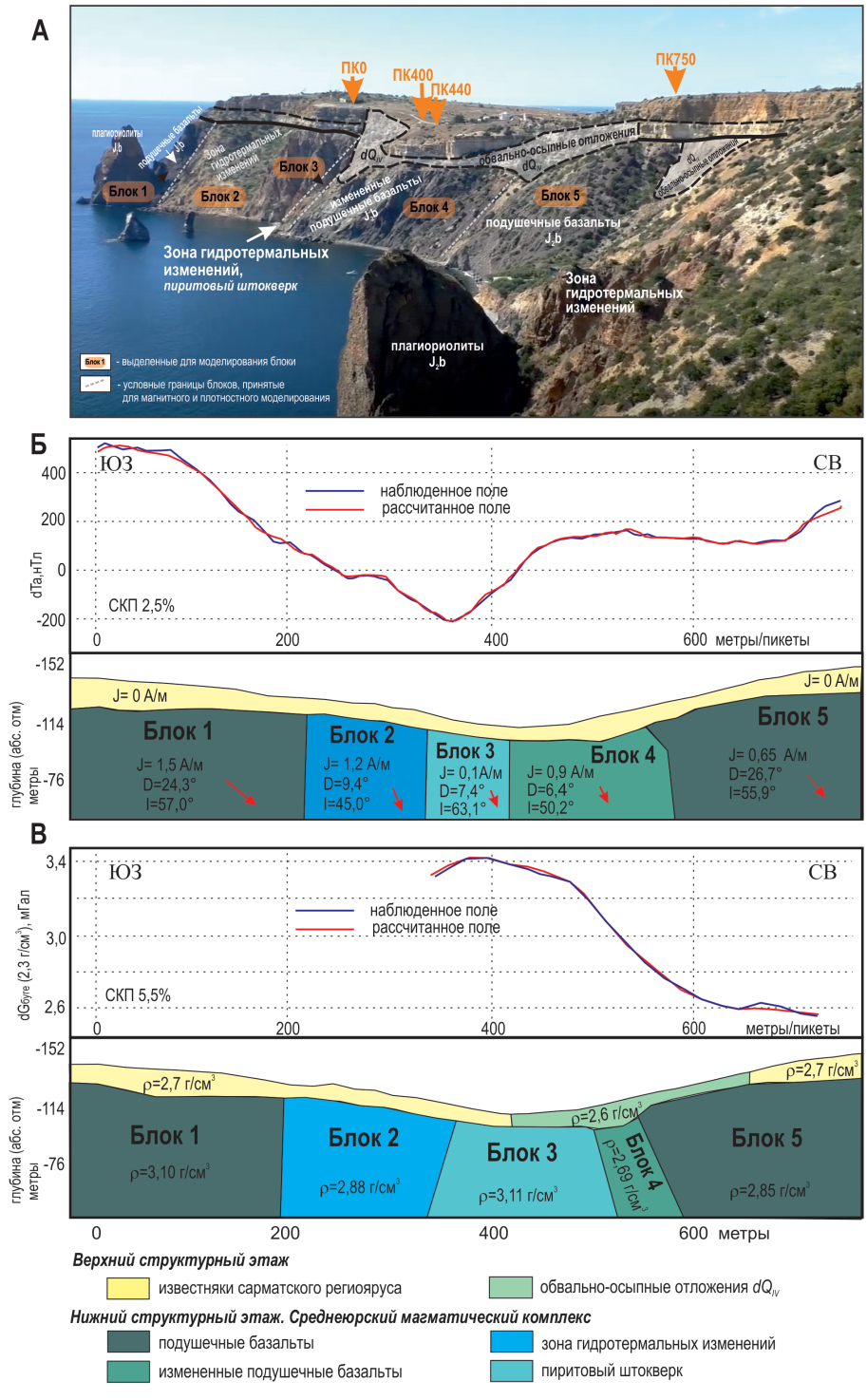

Fig. 8. Photo interpretation of the outcrop on the Cape Fiolent (A) and the results of two-dimensional magnetic (Б) and density (B) modeling in the selection mode along the MMR2 geophysical profile. The numbers on model B show the values of the modulus and the magnetization inclination angle (declination/inclination), the arrows show the projection of the magnetization vector onto the profile line; on B – absolute density values in g/cm³

increases towards the thalweg of the ravine from 3 m in the area of picket 660 in the upper part of the slope of the ravine to 10 m in the area of picket 440, while the conductivity varies from 6.0 Ohm m in the northeast to 1.05 Ohm·m in the thalweg of the ravine (Fig. 9A).

The lower layer has a block structure (Fig. 9). Strong differentiation from 5 to 550 Ohm·m in resistivity in the horizontal direction allows us to distinguish at least 8 blocks with a width from 30 to 160 m (Fig. 9A). The contacts between the blocks dip steeply to the southwest at an angle of 60–70°. Moreover, the farther the block is from the axis of the beam, the higher the resistivity it has. Thus, blocks of high resistivity are located on the extreme southwestern and northeastern sides of the structure, and blocks of medium and low resistivity are located in the center of the beam, near its thalweg.

Directly below the thalweg of the ravine in the area of point 400 at a depth of about 30 m, the section shows a local low-resistivity heterogeneity (resistivity less than 10 Ohm·m) with a width of about 40 m (Fig. 9A). The continuation of this anomalous zone is marked in the form of a jumper that connects the lower and upper conductors into one zone. The same heterogeneity of low resistivity stands out in the area of picket 280, but the width of this heterogeneity is no more than 20 m. The total horizontal size of the zones of medium and low resistivity is 260 m (Fig. 9). This is probably a powerful zone of reworking (and/or weathering), formed in a zone of tectonic disturbance under the influence of processes of abnormal pressure and destruction.

An important feature of the structure of the lower layer is the strong differentiation of individual blocks by resistance. The results obtained indicate that this geological structure is a wide fault zone, which has a width of about 400–500 m and in which individual two-dimensional and three-dimensional blocks of varying degrees of altered rocks are noted.

Discussion and conclusions

As a result of 2D magnetic and gravity modeling, the similarity of the models to each other is shown (Fig. 8Б, В). In this case, the selection of densities and magnetization, as well as the determination of the position and inclination of subvertical boundaries, were carried out within only the lower structural stage, since the magnetization of the rocks of the upper structural stage is two orders of magnitude lower than that of the lower structural stage (Table 2).

Positive magnetic anomalies and the highest values of magnetization and magnetic susceptibility are observed in the least altered pillow basalts. Block 1 is characterized by increased density and magnetization.

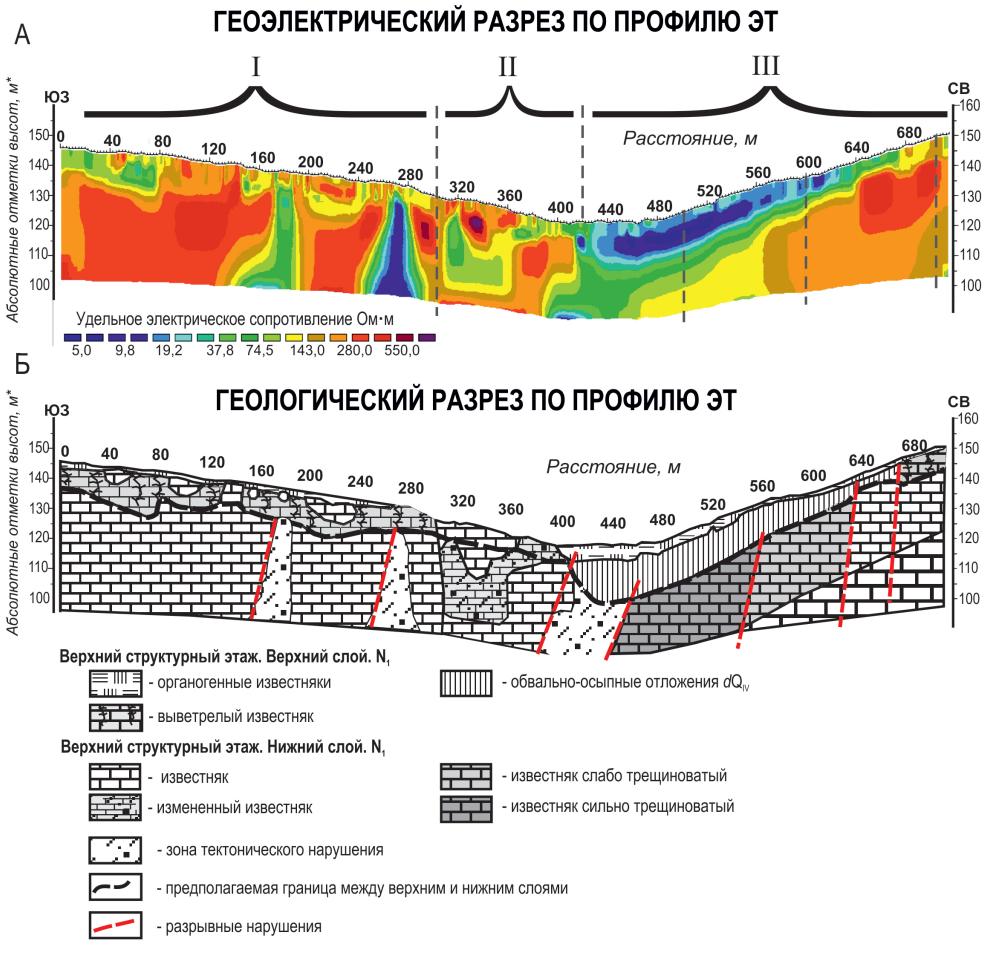

Fig. 9. Geoelectric section (A) and geological (Б) sections along the ET electrical tomography profile on the Cape Fiolent

There is a natural change in the main mineral carrier of magnetization from low-titanium titanomagnetite at a distance from the contact zone of pillow basalts with plagiorhyolites to titanomaghemite with Curie temperatures up to 600–620 °C. Pechersky et al. (1991) associate such changes in the magnetic fraction with low-temperature single-phase oxidation of titanomagnetites (maghemitization). In this case, the ratio of iron cations of different valences changes towards their higher valency while maintaining the crystalline structure of the original mineral as a result of the introduction of oxygen. Another explanation for the appearance of ferric iron is possible. In the presence of seawater, primary titanomagnetites in the main intrusions, as a result of heterophase oxidation, decompose into magnetite and ilmenite at temperatures below 300 °C. Subsequently, ilmenite is oxidized to hematite and anatase. In both cases, changes occur at the postmagmatic stage and the age of the rocks is somewhat different from the time the rocks acquired this component of magnetization. In the density and magnetic models, the block corresponding to the zone of altered pillow basalts (Block 4 in Fig. 8) is characterized by significantly reduced density and magnetization values.

In plagiorhyolites, the value of magnetic susceptibility decreases by 2.5–3 times towards the contact zones, and in the most altered parts χ drops to $(0.1–1.0)\cdot10^{-3}$ SI. At the same time, the density and magnetization to the contact parts of plagiorhyolites decrease. This distribution of magnetic susceptibility in different parts of plagiorhyolite bodies is associated with a change in the composition of the magnetic fraction - in the central parts the main mineral carrier of magnetization is magnetite, while in metasomatites it is monoclinic pyrrhotite.

Negative hydromagnetic anomalies correlate with zones of hydrothermal reworking at the contact of plagiorhyolites and pillow basalts and spatially controlled by NW-trending faults (Fig. 10). Fault zones also correlate well with linearly elongated negative magnetic anomalies (Fig. 10) identified by ground-based magnetometric studies (Pivovarov et al., 1984; Krylov et al., 2023). Magnetic minima in the MMP1–MMP4 and GM2017 profiles are associated with these same zones (Block 2, Fig. 8 and Fig. 10).

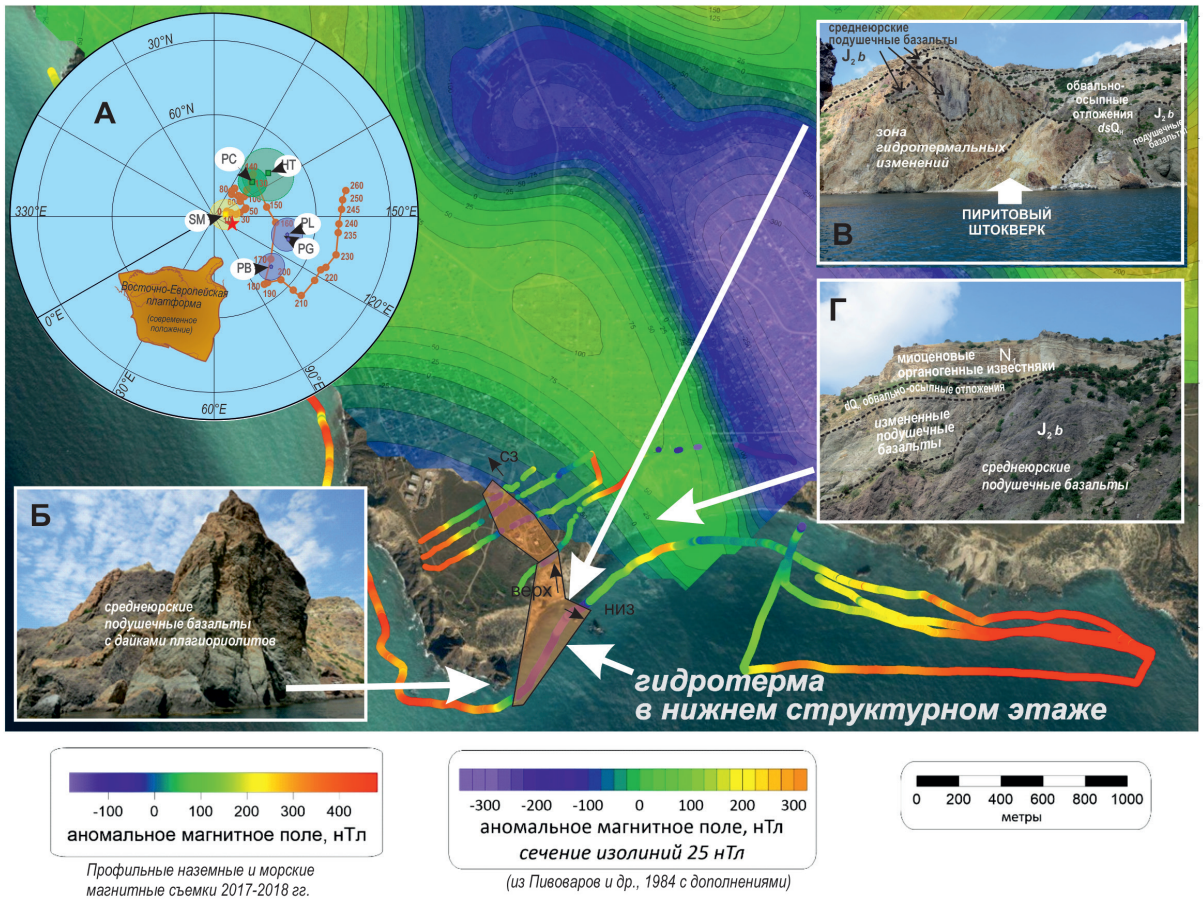

Fig. 10. Map of the anomalous magnetic field (modified after Pivovarov et al., 1984). In the insets: А – magnetization components identified during petro- and paleomagnetic studies on the Cape Fiolent (for letter designations of the components, see Tables 2 and 3) and Apparent Polar Wander Path (APWP) for the East European Platform (modified after Besse, Courtillot, 2003). Projection onto the lower hemisphere. The asterisk indicates the position of the modern geomagnetic pole in the work area. The numbers on APWP are the age of the poles, Ma; Б – Г: deciphered photographs of blocks identified for two-dimensional magnetic and density modeling (Fig. 8, А): Б – block of pillow basalts with plagiorhyolite dikes; В – "pyrite stockwork" (block 3) and Г – altered and unaltered pillow basalts (blocks 4 and 5 in the models, respectively)

In the zone of contact changes, rocks are characterized by reduced values of magnetic susceptibility, lying within the sensitivity of the KT-5, also by reduced densities (2.8 g/cm^3) and magnetization J = 1.2 A/m, D = 9.4°, I = 45.0°.

In samples from the central part of the "pyrite stockwork" (alterated quartzite, Block 3 in Fig. 8), a predominantly paramagnetic fraction containing no remanent magnetization (Q < 1) is found. This block creates the greatest anomalous effect and is characterized by low magnetization (J = 0.1 A/m, D = 7.4°, I = 63.1°), extremely low magnetic susceptibility values ((0.01–0.03) 10^{-3} SI) and high density (3.11 g/cm^3). The main discrepancies in the geometry of the magnetic and gravity models are observed in this area. In the magnetic model, this is a block about 100 m wide and almost vertical contacts, and in the gravity model - trapezoidal shape with a width of 150 meters at the top edge and angles of ~ 60°–70°. Such discrepancies may be due to the different influence of mineralization processes on magnetic and density properties and/or to an increase the hydrothermal alteration with depth. The latter is also supported by longer hydromagnetic anomalies compared to ground ones (Fig. 10).

It should be noted that sharp changes in magnetic susceptibility and negative magnetic anomalies are observed when two conditions are met: (1) contact of pillow basalts with plagiorhyolites and (2) the presence of deep II-order faults of northwest strike. In the absence of deep faults, sulfide ores are not formed and on the hydromagnetic profile such zones are characterized by positive magnetic anomalies (Block 5 in Fig. 8) with magnetization J = 0.65 A/m, D = 26.7°, I = 55.9° and density 2.85 g/cm^3.

The time of existence of the hydrothermal system can be judged only from indirect data. In table Figure 3 shows the paleomagnetic poles, recalculated from the identified magnetization components to the coordinates of sampling points at the Cape Fiolent. The paleomagnetic poles in samples of pillow basalts and plagiorhyolites (components PB and PL in Table 3) are close to the 170–160 Ma pole of the East European Platform (Fig. 10, Inset A).

Taking into account the age of the plagiorhyolites – 168.3 ± 1.3 Ma (Kuznetsov et al., 2022), we accept the age of the characteristic component of magnetization (ChRM) in plagiorhyolites and pillow basalts as Middle Jurassic (Bajocian).

In samples from the hydrothermal alteration zone, a magnetization component was identified that coincides with the ~140 Ma pole for the East European Platform (HT pole in Fig. 10, inset A; Table 3). The close-direction component is identified in the low-medium temperature range as a magnetization reversal component (along a great circle arc) for some samples of predominantly plagiorhyolites, and in rare cases, pillow basalts (Table 3). At the same time, a secondary component of a similar direction is not distinguished in the overlying

Rock type	ID	Polarity	Paleomagnetic pole Φ, °	Λ, °	dp, °	dm, °	φ_m,°	Source
Upper structural level. Miocene limestones of the Sarmatian regional stage								
Limestones	SM	N	86.9	156.0	5.0	6.5	42.8	Present work
Lower structural level. Middle Jurassic igneous complexes								
Pillow basalts	PB	N	70.7	136.1	5.0	6.8	37.6	Present work
Altered pillow basalts	PC	N	75.5	191.1	3.7	5.5	30.9	Present work
	PG	N	67.6	132.2	14.8	20.5	37.4	(Pechersky et al., 1991)
Pillow basalts *(remagnetization circles*	PC_{C1}	–	55.7	136.3	–	–	29.0	(Pechersky et al., 1991)
	PC_{C2}	–	–75.7	61.8	–	–	31.6	(Pechersky et al., 1991)
Plagiorhyolites	PL	N	68.3	136.0	4.7	6.6	36.4	Present work
Hydrothermal alteration zone	HT	N	70.5	187.5	6.1	9.6	26.6	Present work

Table 3. Paleomagnetic poles recalculated from the identified NRM components in the rocks on the Cape Fiolent. Symbols: ID – high-temperature components of magnetization (letter designations, see Table 2); Φ, °, Λ, ° – latitude and longitude of the paleomagnetic pole, respectively; dp and dm are the semi-axes of the paleomagnetic pole confidence oval in degrees; φ_m – paleolatitude in degrees N

Miocene limestones (Table 3). Thus, the hydrothermal system of the Cape Fiolent most likely existed between 168 and 140 Ma.

The short-term existence of the hydrothermal system is also confirmed by the results of thermodynamic modeling carried out earlier for island-arc systems by D.V. Grichuk (2012). According to these data, the action of the island-arc hydrothermal system is limited to the first tens of thousands years.

Sulfide mineralization is limited to the lower structural floor. A layer of anomalously low resistance identified in the upper structural floor at a depth of 3–7 m, dipping at an angle of 6–7° in the SW-direction, is associated with landslide deposits of Miocene bedrock, and not with sulfide mineralization (Krylov et al. , 2023). Previous studies by the IP method at the Cape Fiolent also showed the absence of sulfide mineralization in the upper structural floor (Pivovarov et al., 1984). The results of petro- and paleomagnetic studies also indirectly indicate the absence of sulfides in the upper structural floor. Thermomagnetic analysis data indicate the presence of only greigite and a minor amount of magnetite in the magnetic fraction. In addition, the ChRM components identified in the Miocene limestones and in the zone of hydrothermal alterations of the lower structural level have significant differences in inclination. It should also be noted that the zone of tectonic disturbances in the upper structural floor is displaced by 40–50 m in the NE-direction relative to the fault in the lower structural floor (Krylov et al., 2023).

Thus, the studies showed that the formation of the hydrothermal system occurred in several stages.

(1) At an early stage, plagiorhyolites were intruded into pillow basalts. The bodies of plagiorhyolites became sources of heat, and convective circulation of sea water began around them. During the interaction between water and rock, seawater changed its composition, turning into a hydrothermal fluid. Thus, seawater sulfate was reduced to hydrogen sulfide.

(2) A zone of hydrothermal reworking is observed at the contact between plagiorhyolites and pillow basalts. When hydrothermal fluid interacts with host rocks, a large amount of sulfides, including iron, is formed, with the greatest changes occurring in the contact zone of acidic rocks, since this zone is most permeable to fluids.

(3) Exposure to hydrothermal solutions results in leaching of metals such as copper, zinc and lead. The fluid, saturated with metals, rose along the faults to the surface, where sulfide ores were formed due to cooling. The presence of arsenic pyrite and admixtures of silver and antimony indicate that, in addition to seawater, a magmatic fluid, probably separated from acidic intrusions, was involved in the hydrothermal system.

(4) The interaction of hydrothermal solutions with host rocks led to pyritization and the formation of metasomatic rocks consistent with acid leaching. A wide range of sulfide ores in hydrothermally altered rocks ("pyrite stockwork") suggests that their formation occurred in island-arc systems with convective feeding.

(5) At the same time, the sulfide veins coming to the surface are experiencing active modern weathering. Secondary minerals such as gypsum, jarosite, microsommite, and basaluminite, identified from the results of X-ray phase analysis, are characteristic of the weathering zones of sulfide deposits in the Mediterranean climate.

Conclusion

As a result of the research, hydrothermal transformations of rocks of the Middle Jurassic igneous complex were revealed. A genetic connection between these changes and acidic intrusions has been determined. Metasomatites (up to alterated quartzites) are confined to the contact zone and faults. The mineralization zone contains pyrite, sphalerite, galena, chalcopyrite and pyrrhotite, as well as arsenic pyrite. In the central part, sulfide stockworks are subject to weathering processes and contain significant amounts of secondary sulfates; in the peripheral zones – goethite, which is associated with the amount of hydrothermal pyrite.

The negative magnetic anomaly established during hydromagnetic studies is associated with chemical changes in the main minerals that carry magnetization during hydrothermal changes in the contact part of acidic rocks, since this zone is the most permeable to fluids. The decomposition of primary titanomagnetites in the main intrusions into magnetite and ilmenite is associated with their heterophase oxidation in the presence of sea water at temperatures below 300 °C. Subsequently, ilmenite was oxidized to hematite and anatase. When hydrothermal fluid interacts with host rocks, large amounts of sulfides, including iron, are formed. At the Cape Fiolent, as a result of rock magnetic studies, the presence of at least two of them was established – monoclinic pyrrhotite and pyrite. The best combination of the gravity anomaly obtained during field studies and model calculations is observed precisely in the presence of sulfide (pyrite) mineralization in the marginal part.

The displacement of the magnetic and electrical tomographic anomalies relative to the relief minimum is associated with the inclined dip of the fault zone in the southwestern direction.

As a result of complex studies, a model for the formation of the hydrothermal system of the Cape Fiolent (South-Western Crimea) was proposed.

Acknowledgements

The work carried out within the framework of the SevSU grant "Creation of a digital model of geodynamic environments and environmental monitoring of

hazardous processes in the Sevastopol region" (ID 42-01-09/241/2022-1).

The authors are grateful to Alexei Bubnov and Valentin Osadchii for help in organizing and conducting field studies, Alvina Chistyakova for conducting laboratory petromagnetic studies.

The authors are very grateful to anonymous referees for valuable comments and suggestions that contributed to the improvement of the work.

References

Afanasenkov A.P., Nikishin A.M., Obukhov A.N. (2007). The geological structure and hydrocarbon potential of the Eastern Black Sea region. Moscow: Nauchnyy mir, 172 p. (In Russ.)

Alken P., Thébault E., Beggan C.D. et al. (2021). International Geomagnetic Reference Field: the thirteenth generation. *Earth Planets Space,* 73, p. 49. doi: 10.1186/s40623-020-01288-x

Besse J., Courtillot V. (2003). Correction to "Apparent and true polar wander and the geometry of the geomagnetic field over the last 200 Myr". *Journal of Geophysical Research*, 108 (B10), 2469. https://doi.org/10.1029/2003JB002684

Borisenko L.S., Tikhonenkova E.G., Poltorakov S.V. et al. (1981). Polymetallic manifestations and prospects for the discovery of polymetallic ores in the Crimea. *Geologicheskiy zhurnal*, 1, pp. 12–18. (In Russ.)

Bulychev A.A., Zaitsev A.N. (2008a). A program for interactive two-dimensional selection of a density medium based on an anomalous gravitational field. Certificate of state registration of the computer program No. 2008611947. Issued on 04/18/2008. (In Russ.)

Bulychev A.A., Zaitsev A.N. (2008b). A program for two-dimensional selection of models of magnetized objects based on an anomalous magnetic field. Certificate of state registration of the computer program No. 2008611946. Issued on 04/18/2008. (In Russ.)

Isaev V.S., Koshurnikov A.V., Ignatov E.I. et al. (2018). Coastal Processes: Monitoring and Innovative Integrated Research. Sevastopol: ECOSY-Hydrophysics, 246 p. (In Russ.)

de Ronde C.E.J., Massoth G.J., Butterfield D.A., Christenson B.W., Ishibashi J., Ditchburn R.G., Hannington M.D., Brathwaite R.L., Lupton J.E., Kamenetsky V.S., Graham I.J., Zellmer G.F., Dziak R.P., Embley R.W., Dekov V.M., Munnik F., Lahr J., Evans L.J., Takai K. (2011). Submarine hydrothermal activity and gold-rich mineralization at Brothers volcano, Kermadec arc, New Zealand. *Mineralium Deposita*, 46, pp. 541–584. https://doi.org/10.1007/s00126-011-0345-8

Dvoychenko P.A. (1914). Minerals of the Crimea. A brief essay with a literature review, edited with an introductory article and additions by A.E. Fersman. Simferopol: Zap. Crimean OE, 4, 208 p. (In Russ.)

Fouquet Y., Pelleter E., Konn C., Chazot G., Dupré S., Alix A.S., Chéron S., Donval J.P., Guyader V., Etoubleau J., Charlou J.L., Labanieh S., Scalabrin C. (2018). Volcanic and hydrothermal processes in submarine calderas: The Kulo Lasi example (SW Pacific). *Ore Geology Reviews*, 99, pp. 314–343. https://doi.org/10.1016/j.oregeorev.2018.06.006

Geology of the USSR (1969). Vol. 8. Part 1. Geological description. Moscow: Nedra, 576 p. (In Russ.)

Golubev L.V., Litvinov V.I., Moskalevsky A.T. (1976). Report on the results of electrical, magnetic and seismic exploration in the southwestern part of the Mountainous Crimea (work of KGFP 211/75). KGFP Foundation. (In Russ.)

Grichuk D.V. (2012). Thermodynamic model of ore-forming processes in a submarine island-arc hydrothermal system. *Geochemistry International*, 50, pp. 1069–1100. https://doi.org/10.1134/S0016702912130046

Ivanov V.E., Lomakin I.E., Topolyuk A.S. et al. (2009). Features of the tectonics of the Southwestern Crimea. *Geologiya i poleznye iskopaemye Mirovogo okeana*, (4), pp. 27–39. (In Russ.)

Keith, M., Haase K.M., Häckel, F., Schwarz-Schampera U., Klemd R., Hannington M., Strauss H., McConachy T., Anderson M. (2021). Trace element fractionation and precipitation in submarine back-arc hydrothermal systems, Nifonea caldera, New Hebrides subduction zone. *Ore Geology Reviews*, 135, 104211. https://doi.org/10.1016/j.oregeorev.2021.104211

Khramov A.N., Goncharov G.I., Komissarova R.A. et al. (1982). Paleomagnetology. Leningrad: Nedra, 312 p. (In Russ.)

Kirschvink, J.L. (1980). The least-square line and plane and the analysis of palaeomagnetic data. *Geophysical Journal of Royal Astronomical Society*, 62, pp. 699–718.

Krylov O.V., Lubnina N.V., Vladov M.L., Modin I.N., Bryantseva G.V., Kosevich N.I., Palenov A.Yu., Skobelev A.D., Gushchin A.I., Osadchiy V.O., Evstigneev V.P., Fadeev A.A. (2023). Creation of a Training Site for an Integrated Geological and Geophysical Study of Fracturing in Southwestern Crimea (Cape Fiolent, Heracles Plateau). *Moscow University Geology Bulletin*, 78(1), pp. 153–166. https://doi.org/10.3103/S014587522301012X

Kuznetsov , N. B., Romanyuk , T. V., Strashko , A. V., & Novikova , A. S. (2022). Ophiolite association of Cape Fiolent (western part of the Mountainous Crimea) – the upper age constraint according to the U-Pb isotope dating of plagiorhyolites (Monakh Cliff). Journal of Mining Institute, 255, 435–447. https://doi.org/10.31897/PMI.2022.37

Litvinov V.I., Golubev L.V. (1983). Report on the results of magnetic and electrical exploration in the western part of the Mountainous Crimea (work of KGFP 239/83). KGFP funds. (In Russ.)

Lubnina N.V., Krylov O.V., Bychkov A.Yu. et al. (2021). Innovative Educational Center for Earth Sciences: Major Achievements. *Innovations in Geology, Geophysics and Geography-2021. Proc. 6th International Scientific and Practical Conference*. Moscow: Pero Publishing House, pp. 3–28. (In Russ.)

Lubnina N.V., Krylov O.V., Modin I.N. et al. (2022). Complexing of structural, geomorphological and electrotomographic studies to study the fracturing of Miocene deposits of the Heracleian Plateau (South-Western Crimea). *Geofizika*, (6), pp. 115–120. (In Russ.)

Murovskaya A.V., Shcherbakov R.N. (2011). Structural and kinematic paragenesis and deformation regimes of the Heraclea block of the south-western Crimea. *Nauchnye trudy Donetskogo natsional'nogo tekhnicheskogo universiteta. Seriya gorno-geologicheskaya*, 13(178), pp. 122–128. (In Russ.)

Nikishin, A.M., Okay, A.I., Tüysüz, O., Demirer A., Amelin N., Petrov E. (2015). The Black Sea basins structure and history: New model based on new deep penetration regional seismic data. Part 1: Basins structure and fill. *Marine and Petroleum Geology*, 59, pp. 638–655. https://doi.org/10.1016/j.marpetgeo.2014.08.017

Okay A.I., Şengör A.M.C., Görür N. (1994). Kinematic history of the opening of the Black Sea and its effect on the surrounding regions. *Geology*, 22(3), 267–270. https://doi.org/10.1130/0091-7613(1994)022<0267:KHOTOO>2.3.CO;2

Pechersky D.M., Didenko A.N., Safonov V.A. and others (1991). Petromagnetic and paleomagnetic characteristics of the Middle Jurassic volcanism of the mountainous Crimea. *Izvestia of the USSR Academy of Sciences. Geological series*, (3), pp. 85–104. (In Russ.)

Pivovarov S.V., Tchaikovsky B.P., Chuba B.S. et al. (1984). Report on deep geological mapping at a scale of 1:50000 of the western part of the Crimean Mountains (Heracleian Plateau) for 1982–1984, 2, 225 p. (In Russ.)

Popov S.P. (1913). About some sulfates from the vicinity of the St. George Monastery in the Crimea. *Izv. Imp. AN*, (5), pp. 253–256. (In Russ.)

Promyslova M.Yu., Demina L.I., Bychkov A.Yu. et al. (2014). The nature of magmatism in the Cape Fiolent area (southwestern Crimea). *Moscow University Geology Bulletin*, 69(6), pp. 390–398. (In Russ.)

Promyslova M.Yu., Bryantseva G.V., Demina L.I., Kosevich N.I. (2019). Neotectonic Structures of the Heraklion Peninsula (Southwestern Grimea). *Moscow University Geology Bulletin*, 74(3), pp. 238–245. (In Russ.)

Shatalov A.N. (1999). Modern processes in the southwestern part of Crimea. *DNAN of Ukraine*, (10), pp. 125–128. (In Russ.)

Shnyukov E.F., Lysenko V.I., Kutiy V.A., Shnyukova E.E. (2019). Gold-silver and sulfide mineralization in the rocks of the Heracleian Plateau (Crimea). *Geologiya i poleznye iskopaemye Mirovogo okeana*, (2), pp. 68–86. (In Russ.)

Shnyukova E.E. (2005). Igneous rocks of Cape Fiolent (southwestern Crimea). Proc. International (X All-Russian) petrographic meeting "Petrography of the XXI century", Kola Scientific Center of the Russian Academy of Sciences, Geological Institute, 2, pp. 289–291. (In Russ.)

Stix J., Kennedy B., Hannington M., Gibson H., Fiske R., Mueller W., Franklin J. (2003). Caldera-forming processes and the origin of submarine volcanogenic massive sulfide deposits. *Geology*, 31(4), pp. 375–378. https://doi.org/10.1130/0091-7613(2003)031<0375:CFPATO>2.0.CO;2

Stoffers P., Worthington T.J., Schwarz-Schampera U., Hannington M.D., Massoth G.J., Hekinian R., Schmidt M., Lundsten L.J., Evans L.J., Vaiomo'unga R., Kerby T. (2006). Submarine volcanoes and high-temperature hydrothermal venting on the Tonga arc, southwest Pacific. *Geology*, 34(6), pp. 453–456. https://doi.org/10.1130/G22227.1

Yudin V.V. (1995). Foothill structure of the Crimea. *Geologicheskiy zhurnal*, 4, pp. 115–119. (In Russ.)

Yudin V.V. (2011). Geodynamics of the Crimea. Simferopol: DIAIPI, 336 p. (In Russ.)

Zijderveld, J.D. (1967). A.C. demagnetization in rocks: analysis of results. In: Collinson, D.W., Creer, K.M., Runcorn, S.K. (Eds.), Methods in Paleomagnetism. Elsevier, New York, pp. 254–286.

About the Authors

Natalia V. Lubnina – Dr. Sci. (Geology and Mineralogy), Leading Researcher, Sevastopol State University
33, Universitetskaya st., Sevastopol, 299053, Russian Federation
e-mail: natalia.lubnina@gmail.com

Oleg V. Krylov – Cand. Sci. (Geology and Mineralogy), Associate Professor, Petroleum Geology Department, Lomonosov Moscow State University
1, Leninskie gory, Moscow, 119234, Russian Federation
e-mail: o.crylov2010@yandex.ru

Andrey Yu. Bychkov – Dr. Sci. (Geology and Mineralogy), Professor, Department of Geochemistry, Lomonosov Moscow State University
1, Leninskie gory, Moscow, 119234, Russian Federation
e-mail: bychkov@geol.msu.ru

Igor N. Modin – Dr. Sci. (Geology and Mineralogy), Professor, Department of Geophysical Methods of the Earth's Crust Studying, Lomonosov Moscow State University
1, Leninskie gory, Moscow, 119234, Russian Federation
e-mail: imodin@yandex.ru

Aleksey D. Skobelev – Engineer, Department of Geophysical Methods of the Earth's Crust Studying, Lomonosov Moscow State University
1, Leninskie gory, Moscow, 119234, Russian Federation
e-mail: askobelev.msu@gmail.com

Elena V. Kozlova – Cand. Sci. (Geology and Mineralogy), Senior Researcher, Hydrocarbons Production Centre, Skolkovo Institute of Science and Technology
3, Nobel st., Moscow, 143026, Russian Federation
e-mail: e.kozlova@skoltech.ru

Maria V. Kosnyreva – Cand. Sci. (Geology and Mineralogy), Associate Professor, Department of Geophysical Methods of the Earth's Crust Studying, Lomonosov Moscow State University
1, Leninskie gory, Moscow, 119234, Russian Federation
e-mail: m.kosnyreva@yandex.ru

Vladimir L. Kosorukov – Cand. Sci. (Geology and Mineralogy), Senior lecturer, Department of Oil and Gas Sedimentology and Marine Geology, Lomonosov Moscow State University
1, Leninskie gory, Moscow, 119234, Russian Federation
e-mail: kosorukov-vladimir@rambler.ru

Nataliia I. Kosevich – Cand. Sci. (Geology and Mineralogy), Associate Professor, Department of Dynamic Geology, Lomonosov Moscow State University
1, Leninskie gory, Moscow, 119234, Russian Federation
e-mail: nkosevich@googlemail.com

Andrey Yu. Palenov – Assistant, Department of Geophysical Methods of the Earth's Crust Studying, Lomonosov Moscow State University
1, Leninskie gory, Moscow, 119234, Russian Federation
e-mail: palenov@mail.ru

Manuscript received 9 December 2022;
Accepted 12 December 2023;
Published 30 March 2024

IN RUSSIAN

Особенности сульфидной минерализации гидротермальной системы мыса Фиолент (юго-западный Крым)

Н.В. Лубнина[1], О.В. Крылов[1,2], А.Ю. Бычков[2], И.Н. Модин[2], А.Д. Скобелев[2], Е.В. Козлова[3], В.Л. Косоруков[2], М.В. Коснырева[2], Н.И. Косевич[1,2], А.Ю. Паленов[2]*

[1]*Севастопольский государственный университет, Севастополь, Россия*
[2]*Московский государственный университет имени М.В. Ломоносова, Москва, Россия*
[3]*Сколковский институт науки и технологий, Москва, Россия*
[*] *Ответственный автор: Наталия Валерьевна Лубнина, e-mail: natalia.lubnina@gmail.com*

Обобщены результаты геофизических исследований, петро- и палеомагнитного и структурно-геоморфологического анализов, позволивших выявить некоторые особенности рудообразования в гидротермальной системе мыса Фиолент (юго-западный Крым) в условиях островной дуги. Установлено, что основные преобразования пород среднеюрского магматического комплекса мыса Фиолент произошли под влиянием гидротермальных флюидов при внедрении интрузивов кислого состава в интервале 168–140 млн лет. Зоны содержат сульфидную минерализацию, основными составляющими которой являются пирит, сфалерит, пирротин, галенит, халькопирит и мышьяковистый пирит. В центральных частях зоны гидротермальных изменений массивные сульфиды сильно выветрены и содержат много вторичных сульфатов. В краевых частях в гипергенном лимоните в зоне окисления преобладает желто-коричневый гётит, в центре – желтый ярозит, что обусловлено, скорее всего, бóльшим количеством пирита в центре штокверка, при окислении которого выделялось больше серной кислоты. Нахождение в разрезе самородной серы свидетельствует о смешении гидротермального раствора с морской водой. Комплексные петро- и палеомагнитные и магнитометрические исследования позволили установить, что контактовые изменения и преобразование контрастной базальт-риолитовой формации происходили по разломам ССЗ-простирания.

Ключевые слова: гидротермальная система, сульфидная минерализация, петро- и палеомагнетизм, электротомография, магнитометрия, разломные зоны, островная дуга

Для цитирования: Лубнина Н.В., Крылов О.В., Бычков А.Ю., Модин И.Н., Скобелев А.Д. , Козлова Е.В. , Косоруков В.Л., Коснырева М.В., Косевич Н.И., Паленов А.Ю. (2024). Особенности сульфидной минерализации гидротермальной системы мыса Фиолент (юго-западный Крым). *Георесурсы,* 26(1), с. 20–37. https://doi.org/10.18599/grs.2024.1.2